ELSEVIER

Journal of Chromatography A, 855 (1999) 57–70

JOURNAL OF CHROMATOGRAPHY A

www.elsevier.com/locate/chroma

On the possibility of shear-driven chromatography: a theoretical performance analysis

Gert Desmet*, Gino V. Baron

Vrije Universiteit Brussel, Department of Chemical Engineering, Pleinlaan 2, 1050 Brussels, Belgium

Received 25 February 1999; received in revised form 11 May 1999; accepted 21 May 1999

Abstract

The use of shear forces for the generation of the mobile phase flow in chromatographic separations is proposed. This novel chromatographic operating principle, referred to as shear-driven chromatography (SDC), completely circumvents the pressure-drop limitation of conventional pressure-driven GC and LC without affecting the operational flexibility (choice of mobile and stationary phases, possibility of solvent and/or temperature programming, etc.). In the present paper, the expression for the height equivalent to a theoretical plate in SDC in a channel with a flat rectangular cross-section is established and is used to demonstrate the large gain in analysis speed under LC, GC and supercritical fluid chromatography conditions.

Keywords: Shear-driven chromatography; Mobile phase flow

1. Introduction

Presently, all chromatographic analysis techniques are either pressure-driven or electrically-driven [1]. The two most popular versions of pressure-driven chromatography are packed-column high-performance liquid chromatography (HPLC) and open-tubular gas chromatography (capillary GC). Although it has recently been demonstrated that HPLC columns can be operated at much more elevated pressures [2,3], mechanical sealing problems, thermal problems and pressure-dependent retention effects usually limit the operating pressure to about 200 to 400 bar for LC. For GC, this pressure-drop is usually limited to 5 to 100 bar (depending upon the gas–liquid equilibrium characteristics of the carrier fluid and the sample). Both in packed and open-tubular columns, this pressure-drop limitation restricts the applicable mobile phase velocity, the column length, and, as a consequence, also the achievable number of theoretical plates. It also puts a down-limit to the column diameter d (open-tubular columns) or particle diameter d_p (packed columns) which can be used to perform a given separation [4]. Considering that the analysis time varies according to d^2 or d_p^2 [5], this diameter down-limit also puts a down-limit on the analysis time. In electrically-driven separations, a similar down-limit exists. In this case, the analysis time is limited by the existence of a maximal allowable voltage drop [6].

2. Shear-driven chromatography (SDC)

As a means to break through these analysis time

*Corresponding author. Tel.: +32-2-6293-251; fax: +32-2-6293-248.

E-mail address: gedesmet@vub.ac.be (G. Desmet)

0021-9673/99/$ – see front matter
PII: S0021-9673(99)00652-4

down-limits, the present study proposes the use of shear forces for the generation of the mobile phase flow. Whereas in pressure-driven chromatography (PDC) the mobile phase flow is generated by applying a (pressure) force at the channel inlet only, the concept of shear-driven chromatography (SDC) is based upon the application of a flow generating (shear) force all along the channel length. In this way, the fluid motion is sustained all along the channel length and the chromatographic operation can be effectuated without the need to impose a pressure gradient. An example of such a shear-driven flow is the parallel plate flow (Couette flow), which is described in nearly every basic text book on hydrodynamics and which is often used to explain the viscous effect of liquids and gases. The absence of a pressure drop can also be understood from the working principle of a so-called viscous pump [7].

Although a wide variety of other layouts can be proposed [8], the most simple and illustrative SDC apparatus consists of a moving belt sliding past a stationary plate in which a straight, flat rectangular channel is recessed (Fig. 1a) which accommodates a stationary phase layer on its bottom wall (Fig. 1b). In this set-up, the moving belt drags the mobile phase fluid in, through and out the separation channel. The required parallelism between moving and stationary channel wall parts can be ensured by firmly pressing the moving belt against the stationary plate and all kind of measures can be taken [8] to provide the moving wall part with a sufficient mechanical transversal rigidity. As the absence of a pressure drop implies that the pressure in each point inside the channel can be kept identical to the surrounding pressure, it is obvious that the danger of a convective leakage flow through the channel side-walls is completely excluded.

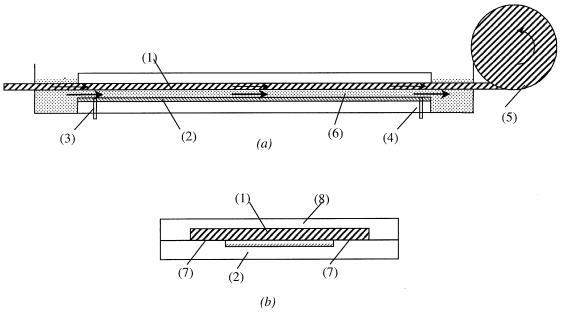

Fig. 1. Possible layout for SDC apparatus: (a) longitudinal view, (b) cross-sectional view. Description of the different parts: (1) moving wall element, (2) stationary wall element carrying the stationary phase layer, (3) injection section, (4) detection section, (5) drive-system for moving wall element, (6) mobile phase fluid, (7) side-banks, (8) cover plate.

A series of preliminary tracer flow experiments has already been conducted with a 2.54 cm long channel arranged stationary glass plate. These experiments successfully demonstrated the feasibility of SDC between two flat plates. It was found that the injected tracer pulse moves with exactly half the speed of the moving plate [cf. Eq. (2)] and that the injected tracer pulse only minimally broadens during its travel along the channel. A more complete report on these experiments will be presented in a following paper.

Fig. 2 clearly illustrates the major difference between SDC and PDC. In open-tubular PDC, a parabolic velocity profile is established (Fig. 2a), and the mean mobile phase (u_m), the column length (L) and the column diameter (d) are restricted by Poiseuille's law:

$$\Delta P_{max} = \frac{\psi \mu u_m L}{d^2} \quad (1)$$

In SDC, a linear velocity profile is established (Fig. 2b) and, as there is no pressure drop, the values of u, d and L can be freely selected. This offers the possibility to design channels yielding thus far unachievable plate numbers (by using large L) and/or yielding extremely fast separations kinetics (by using small d). The latter possibility complies per-

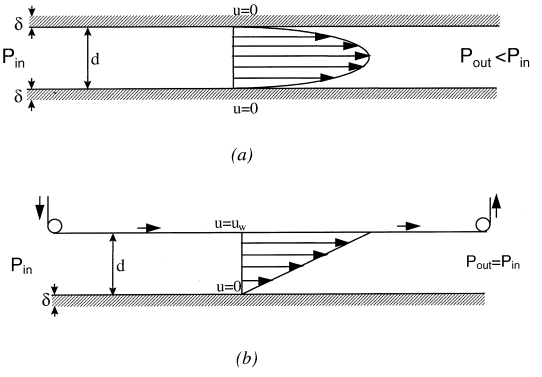

Fig. 2. Flow profiles in PDC (a) and SDC (b).

fectly with recent breakthroughs in the micro-machining and micro-replication technology [9], which allow to envision the manufacturing of a 0.1 μm thick, 100 μm wide and 10 cm long channel with an over-all channel thickness tolerance below 1% [10]. Another important advantage of the concept is that the need for a high-pressure pump is eliminated.

Although the SDC principle can also be exploited in channels with a small aspect ratio cross-section (e.g., a cylindrical or a square-like cross-section), the present study is entirely focused on channels with a flat rectangular cross-section, i.e., channels in which the channel width w is orders of magnitude larger than the channel thickness d. In large aspect ratio channels, the small thickness should provide the fast separation kinetics whereas the much larger width should provide a sufficient optical path length and a sufficient volumetric flow-rate and mass loadability. The use of large aspect-ratio channels to increase the concentration detectability of open-tubular separations has already been investigated for PDC and capillary electrophoresis [5,11,12], but as will be demonstrated, the idea has a much larger chance of being successful with the SDC principle.

3. Calculation of the height equivalent to a theoretical plate (HETP)

To properly evaluate the potential of a chromatographic system, the relation between the HETP and the mobile phase velocity (u) has to be known. As this relation is not at hand for SDC, it has to be derived from Aris' general solution [13]. The HETP calculation for the actual rectangular channel problem will however only be performed in Section 3.2, because we found it instructive to first consider the case of a shear-driven flow between two flat parallel surfaces with an infinite width, i.e., in a hypothetical side-wall-less channel.

3.1. Shear-driven flow between two flat parallel plates

Considering the flow between two infinitely wide and flat parallel plates, one of which is at rest while the other is moving in its own plane with a velocity u_w, and assuming that there is no externally imposed pressure difference, pure hydrodynamic considerations [14] show that the fluid velocity is purely uni-dimensional and varies in a strictly linear way with the distance between the stationary and the moving plate (Fig. 2b):

$$u(y) = u_w y/d \text{ and } u_m = u_w/2 \tag{2a}$$

Or, after introducing the dimensionless variables y ($=y/d$) and u ($=u/u_w$):

$$u = y \text{ and } u_m = 1/2 \tag{2b}$$

Before the HETP calculation can be performed, it should first be noted that Aris' general solution procedure is only valid for axisymmetrical systems. This follows from the condition of a zero net flux across the channel center ($dn/dr = 0$ at $r = r_i$) which is imposed in Aris' original paper [13]. The present flow system therefore first has to be transformed into an equivalent axisymmetrical system. This can however simply be achieved by mirroring the flow system with respect to the moving wall. In this way, the single-side coated flow system with thickness d (Fig. 2b) is replaced by a two-side coated flow system with thickness $2d$ (Fig. 3a). As is shown in Section A.2, the mobile phase mass transfer term ($HETP_m$) for the flow system depicted in Fig. 3a can be calculated to be:

$$HETP_m = \frac{2}{30} \cdot \frac{1 + 7k' + 16k'^2}{(1 + k')^2} \cdot u_m \cdot \frac{d^2}{D_m} \tag{3}$$

From the condition of symmetry across the channel's mid-plane, which is equivalent to the condition of a zero net flux of sample species, it follows directly that the expression given in Eq. (3) is also valid for the actual SDC flow system depicted in Fig. 2b.

To validate Eq. (3), we have compared it to some of the $HETP_m$ expressions known from literature [15] for other flow types. Two flow types are considered: a parabolic, pressure-driven flow between two parallel plates with infinite width (Fig. 3b), and a hypothetical flow with a uniform velocity (Fig. 3c): parabolic flow [15]:

$$HETP_m = \frac{2}{210} \cdot \frac{1 + 9k' + 25.5k'^2}{(1 + k')^2} \cdot u_m \cdot \frac{d^2}{D_m} \tag{4a}$$

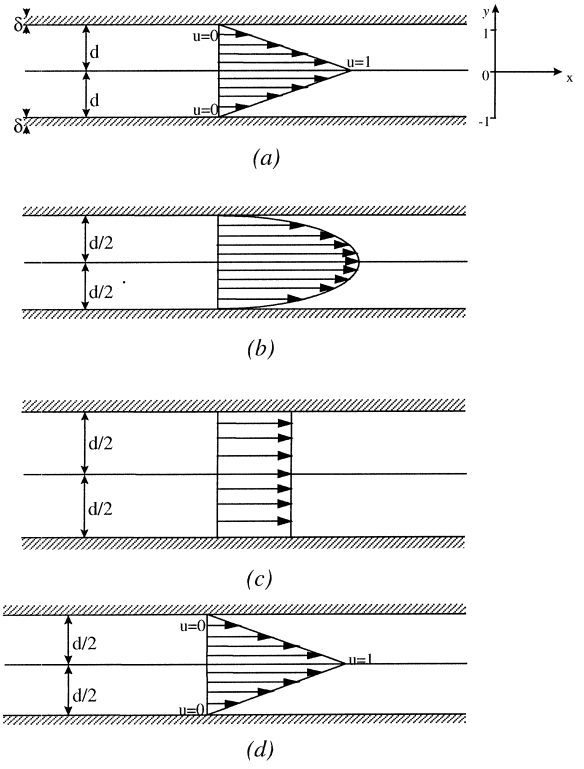

Fig. 3. Different flow systems: (a) double, axi-symmetric SDC flow in channel with diameter 2*d*, (b) parabolic PDC flow, (c) hypothetical, uniform velocity flow, (d) double, axi-symmetric SDC flow in channel with diameter *d*.

and uniform flow [15]:

$$\mathrm{HETP_m} = \frac{2}{6} \cdot \frac{k'^2}{(1+k')^2} \cdot u_\mathrm{m} \cdot \frac{d^2}{D_\mathrm{m}} \qquad (4b)$$

To allow for a proper comparison, it should first be noted that in Eqs. (4a) and (4b) *d* refers to the diameter of the channel, whereas *d* refers to the radius of the channel (i.e., one half of the channel thickness, see Fig. 3a) in the SDC expression [Eq. (3)]. To account for this, the $\mathrm{HETP_m}$ value given in Eq. (3) should first be transposed to the SDC flow system shown in Fig. 3d, with a total diameter (thickness) of *d* instead of 2*d*:

$$\mathrm{HETP_m} = \frac{2}{30} \cdot \frac{1+7k'+16k'^2}{(1+k')^2} \cdot u_\mathrm{m} \cdot \frac{(d/2)^2}{D_\mathrm{m}} = \frac{2}{120} \cdot \frac{1+7k'+16k'^2}{(1+k')^2} \cdot u_\mathrm{m} \cdot \frac{d^2}{D_\mathrm{m}} \qquad (5)$$

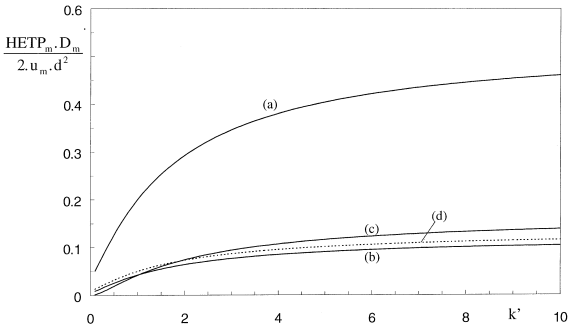

Fig. 4. Normalized $\mathrm{HETP_m}$ values for the different flow systems depicted in Fig. 3. Lettering of the curves as in Fig. 3.

In Fig. 4, the $\mathrm{HETP_m}$ expressions for the different considered flow systems are represented as a function of k', clearly showing that the equivalent SDC system depicted in Fig. 3d yields $\mathrm{HETP_m}$ values (cf. curve d) which are of the same order as that of the two other flows: the difference with the parabolic pressure-driven flow (curve b) is nowhere significantly larger than the difference between the parabolic flow and the uniform flow (curve c). This is in agreement with what can be physically expected and can hence be considered as a validation for Eq. (5) and hence also for Eq. (3).

Returning now to the practical chromatographic system, it should be noted that the flow depicted in Fig. 3a and d only exists in theory, because it would require the movement of an infinitely thin, fully permeable mechanic device along the center plane of the channel. As this cannot be realized in practice, the relevant SDC flow configuration hence corresponds to Fig. 2b, and the relevant $\mathrm{HETP_m}$ expression for SDC in a channel with thickness *d* is hence given by Eq. (3). The proper comparison between SDC and PDC, both in an infinitely wide channel with thickness *d*, should hence occur by comparing Eq. (3) and (4a), or equivalently, by comparing curves (a) and (b) in Fig. 4. The large difference between both $\mathrm{HETP_m}$ curves can now be explained by the fact that, whereas in PDC the stationary phase layer can be applied on both the bottom and the upper wall, the stationary phase layer can only be applied on one of both walls in SDC. As a consequence, the mean radial distance traveled by the sample species during their stay in the mobile phase is doubled, and this explains the large $\mathrm{HETP_m}$ values. As will be shown in Section 4, the unfavorable

$HETP_m$ values of SDC can however easily be countered by the fact that the SDC concept allows a free selection of the channel thickness d, such that it is always possible to select a d value which is sufficiently smaller than the best possible d value which can be used in PDC.

As demonstrated by Giddings [15], the HETP contribution of the stationary phase mass transfer resistance ($HETP_s$) is independent of the mobile phase flow. As the stationary phase in the flat rectangular SDC channel depicted in Fig. 2b is a simple flat slab with thickness δ, the $HETP_s$ value is given by [15]:

$$HETP_s = \frac{2}{3}\cdot\frac{k'}{(1+k')^2}\cdot u_m\cdot\frac{\delta^2}{D_m} \quad (6)$$

Finally, adding all HETP contributions, and including the mobile phase axial diffusion effect, it can be concluded that the global HETP expression for the flow system in Fig. 2b is given by:

$$HETP = 2\cdot\frac{D_m}{u_m} + \frac{2}{30}\cdot\frac{1+7k'+16k'^2}{(1+k')^2}\cdot u_m\cdot\frac{d^2}{D_m} + \frac{2}{3}\cdot\frac{k'}{(1+k')^2}\cdot u_m\cdot\frac{\delta^2}{D_s} \quad (7)$$

3.2. Shear-driven flow in a flat rectangular channel with finite lateral width

Returning now to the case of a closed rectangular channel with finite lateral dimensions, it should be noted that, for the case of a pressure-driven flow, Golay [16], Doshi et al. [17], and many others have demonstrated the unexpectedly large influence of the side-walls. They found that the $w/d\to\infty$-limit of their axial dispersion solution did not reduce to the solution for the infinite wide channel given by Eq. (4a). Instead, they found that the side-walls yield a peak broadening effect, which can be represented by an additional HETP contribution ($HETP_{m,sw}$). In the case of a retentive-less flow, this contribution could be calculated to be [16]:

$$HETP_{m,sw} = 2\kappa_{sw}u_m\cdot\frac{(d/2)^2}{D_m} = 0.0662u_m\cdot\frac{d^2}{D_m}\ (\kappa_{sw}=0.1324) \quad (8)$$

Adding this term to the HETP expression for the side-wall-less case, the HETP for open-tubular PDC in a flat rectangular channel with a finite width is given by:

$$HETP = \frac{2D_m}{u} + 2u\cdot\frac{1+9k'+25.5k'^2}{210(1+k')^2}\cdot\frac{d^2}{D_m} + \frac{2}{3}\cdot\frac{k'}{(1+k')^2}\cdot u_m\cdot\frac{\delta^2}{D_s} + 0.0662u_m\frac{d^2}{D_m} \quad (9)$$

Experimental evidence for Eq. (9) has been gathered by Martin et al. [19]. Grouping the axial dispersion terms, Eq. (9) can be rewritten to yield Eq. (T4b) of Table 1. Eq. (9) shows that, in the case of a retentive-less flow with $u_m \gg u_{opt}$, the presence of the side-walls increases the HETP by a factor of 7.94 as compared to the side-wall-less case [16,18].

As the side-wall effect leads to a severe deterioration of the PDC performance [16], it is obvious that the side-wall effect also has to be investigated for the SDC case. To properly assess this effect, Aris' general solution procedure has to be applied to the three-dimensional (3D) velocity profile induced by the presence of the side-walls in the SDC channel (see Fig. 5a–b). This constitutes a very difficult calculation problem. But, for the case of a large aspect ratio cross-section (i.e., $w \gg d$), the problem can be considerably simplified by approximating the actual 3D velocity field by the 2D velocity field which is obtained when averaging the actual velocity field over the y-direction. This approximation is justified because, in channels with a large aspect ratio, the differences in mobile phase velocity are much more rapidly equilibrated across the channel thickness than across the channel width. The validity of this approximate approach has been largely discussed and demonstrated by Cifuentes and Poppe [20] for both PDC and capillary zone electrophoresis in flat rectangular channels.

The full calculation of the additional side-wall contribution for the SDC flow is given in Appendix A.2, yielding:

$$HETP_{m,sw} = 2\kappa_{sw}u_m\cdot\frac{(d/2)^2}{D_m} = 0.04945u_m\cdot\frac{d^2}{D_m} \quad (10)$$

Table 1
HETP expressions

I. HPLC [4]:	$\mathrm{HETP} = A \cdot d_p + B \cdot \frac{D_m}{u} + Cu \cdot \frac{d_p^2}{D_{mol}}$	(T1)
	with: $A = 2\lambda$ ($\lambda = 0.5$) $B = 2\gamma$ ($\gamma = 0.8$) $C = \frac{0.37 + 4.69k' + 4.04k'^2}{(1+k')^2 D_m}$	
II. Open-tubular chromatography:	$\mathrm{HETP} = \frac{2D_m}{u} + 2uf' \cdot \frac{d^2}{(1+k')D_m}$	(T2)
IIa. PDC (cylindrical capillary) [15]:	$f' = \frac{1}{192} \cdot (1 + 6k' + 11k'^2) + \frac{\phi^2}{3\epsilon} \cdot k'$	(T3)
IIb. PDC (flat rectangular channel) [15]:	$f' = \frac{1}{210} \cdot (a + 9k' + \frac{51}{2}k'^2) + \frac{\phi^2}{3\epsilon} \cdot k'$	(T4)
No side-wall:	$a = 1$	(T4a)
With side-wall:	$a = 7.94$	(T4b)
IIb. SDC (flat rectangular channel):	$f' = \frac{1}{30} \cdot (a + 7k' + 16k'^2) + \frac{\phi^2}{3\epsilon} \cdot k'$	(T5)
No side-wall:	$a = 1$	(T5a)
With side-wall:	$a = 1.74$	(T5b)

Adding this term to Eq. (16), the following global HETP expression for SDC in a flat rectangular channel with a large, but finite lateral width ($w \gg d$) is obtained:

$$\mathrm{HETP} = \frac{2D_m}{u_m} + 2u_m \cdot \frac{1 + 7k' + 16k'^2}{30(1+k')^2} \cdot \frac{d^2}{D_m} + \frac{2}{3} \cdot \frac{k'}{(1+k')^2} u_m \frac{\delta^2}{D_s} + 0.0494 u_m \frac{d^2}{D_m} \quad (11)$$

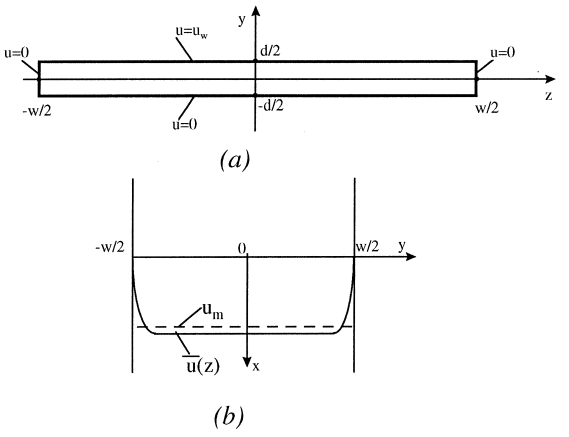

Fig. 5. Schematic representation of SDC in a channel with side-walls: boundary conditions (a) and averaged axial velocities $\bar{u}(z)$ and u_m (b).

Similar to Eq. (9), Eq. (11) can also be rewritten by grouping the axial dispersion terms. This yields Eq. (T5b) of Table 1. Comparing Eq. (10) to Eq. (8), it can be seen that the side-wall effect in SDC is somewhat smaller, but still of the same order of magnitude as in PDC. However, as the basic HETP_m contribution (i.e., for the side-wall-less case) is significantly larger for SDC than for PDC, it is obvious that the relative increase of the axial dispersion caused by the side-walls is much less important for SDC than for PDC (see also Fig. 7). For a retentive-less, high-velocity SDC flow, this increase is equal to $(0.0494 + 2/30)/(2/30) = 1.74$, which is obviously much smaller than the factor of 7.94 [17] for the corresponding PDC case.

4. Comparison with pressure-driven LC [high-performance liquid chromatography/open-tubular liquid chromatography (HPLC/OT-LC)]

With the HETP expressions derived in the previous Section, the separation speed of SDC can now be compared to that of the conventional PDC systems, using:

$$t_{anal} = \frac{N \cdot \mathrm{HETP}}{u_m} \cdot (1 + k') \tag{12}$$

and:

$$N = \frac{16R_s^2}{(1-\alpha_s)^2} \cdot \frac{(1+k')^2}{k'^2} \tag{13}$$

The HETP expressions for the different considered chromatographic flow systems are summarized in Table 1. In Eq. (13), α_s is the separation factor for two members of a given critical pair, R_s is the desired degree of resolution and k' refers to the retention factor of the first eluting component of the critical pair ($m=\phi$). For PDC, the mobile phase velocity u is limited by Poiseuille's law ($d=d_p$ for packed column PDC):

$$\Delta P_{max} = \frac{\psi\mu u_m \cdot N \cdot \mathrm{HETP}}{d^2} \tag{14}$$

For SDC, the mobile phase velocity u_m can be freely selected. However, just as for PDC, an optimal mobile phase velocity u_{opt} can be identified from the minimum of the (HETP, u_m) relationship. As the HETP expression for SDC is of the form [cf. Eqs. (T5a) and (T5b) in Table 1]:

$$\mathrm{HETP} = \frac{2D_m}{u_m} + 2u_m C \tag{15}$$

it can easily be shown that:

$$\mathrm{HETP} = \mathrm{HETP}_{min} \Leftrightarrow u_m = u_{opt} = \sqrt{\frac{D_m}{C}} \tag{16}$$

Inserting Eq. (16) into Eq. (15), it follows readily that:

$$\mathrm{HETP}_{min} = 4\sqrt{D_m C} \tag{17}$$

From Eqs. (12), (16) and (17) it can easily be verified that:

$$t_{anal,opt} = 4NC(1+k') = 4Nf' \cdot \frac{d^2}{D_m} \cdot (1+k') \tag{18}$$

The f' factor is defined according to $C=f'd^2/D_m$ in Eq. (T2) of Table 1. Eq. (18) yields the analysis time for the $u_m=u_{opt}$ case, i.e., the case yielding the minimal HETP and minimal column length conditions. The analysis time can however be further decreased by increasing u_m above u_{opt}. Putting $u_m=\infty$ in Eqs. (12) and (15), and calculating the corresponding analysis time, it is easily found that:

$$t_{anal,min} = 2NC(1+k') = 2Nf' \cdot \frac{d^2}{D_m} \cdot (1+k') \tag{19}$$

This value is exactly one half of the t_{anal} value given by Eq. (18). It can be shown that this ultimate separation speed is already sufficiently approximated from about $u_m=10u_{opt}$ on. For the SDC case, the $u_m=u_{opt}$ and the $u_m \gg u_{opt}$ velocities can unconditionally be imposed, and Eqs. (18) and (9) are always valid. Provided that the pressure drop limitation is not violated, the results and conclusions represented by Eqs. (15)–(19) are in fact also valid for PDC. However, when exploring the performance limits of SDC and PDC, the pressure drop limitation of PDC inevitably comes into play. For open-tubular PDC, this limitation is reflected by the existence of an optimal column diameter (d_{opt}), which is, independently of the channel geometry, given by [21]:

$$d_{opt}^2 = \frac{4\psi\mu D_m N}{\Delta P_{max}} \tag{20}$$

For packed column PDC, a fully similar expression can be established for the optimal particle diameter $d_{p,opt}$ [4]. Eq. (20) expresses the well known fact that the absolute minimal analysis time under PDC conditions is obtained for the column or particle diameter for which the corresponding u_{opt} velocity exactly yields the maximal allowable pressure drop in a column which is exactly long enough to yield the desired plate number. This implies that in PDC a different optimal column or particle diameter prevails for each different separation. It also implies that the absolute minimal analysis time for PDC is given by Eq. (18), after replacing d by d_{opt} [Eq. (20)], and after replacing u_m by u_{opt} [Eq. (16)]:

$$t_{\text{anal,min}}(\text{PDC}) = 16 \cdot \frac{\psi\mu}{\Delta P_{\max}} \cdot N^2 f'(1+k') \tag{21}$$

or:

$$t_{\text{anal,min}}(\text{PDC}) \sim N^2 \tag{22}$$

For SDC, Eqs. (18) and (19) remain unconditionally valid, and hence:

$$t_{\text{anal,min}}(\text{SDC}) \sim N \tag{23}$$

Comparing Eqs. (22) and (23) immediately shows that the most marked advantage of SDC lies in the fact that it allows to select the column diameter d independently of N, such that $t_{\text{anal,min}}$ increases in a directly proportional way with N, whereas in PDC, an increase of the required theoretical plate number also implies an increase of the optimal column or particle diameter, such that $t_{\text{anal,min}}$ increases according to N^2. The advantage of SDC will hence be most pronounced for separations requiring large N values. However, SDC is also advantageous for more routine-like separations, because it allows the use of d values which are much smaller than the optimal d value for the corresponding PDC case. As t_{anal} varies according to d^2 [cf. Eqs. (18) and (19)], the advantage is obvious.

When comparing the analysis times of different chromatographic systems, it should also be considered that a different optimal retention factor ($k' = k'_{\text{opt}}$) can be identified for each of these systems. This k'_{opt} value corresponds to the value of k' for which the $t_{\text{anal,min}}$ expressions given in Eqs. (22) and (23) reach their minimum. For the PDC case, considering Eq. (21), and replacing N by its relation to k' [Eq. (13)], the following relation between $t_{\text{anal,min}}$ and k' is obtained:

$$t_{\text{anal,min}}(\text{PDC}) = \frac{64^2 R_s^4}{(1-\alpha_s)^4} \cdot \frac{\psi\mu}{\Delta P_{\max}} \cdot f'(k') \cdot \frac{(1+k')^3}{k'^4} \tag{24}$$

For the SDC case, the relation between $t_{\text{anal,min}}$ and k' is simply obtained by replacing N by its relation to k' in Eq. (18):

$$t_{\text{anal,min}}(\text{SDC}) = \frac{64 R_s^2}{(1-\alpha_s)^2} \cdot f'(k') \cdot \frac{(1+k')}{k'^2} \cdot \frac{d^2}{D_m} \tag{25}$$

Eqs. (24) and (25) are both clearly optimizable with respect to k'. As the numeric constants in the expression for f' are different for each chromatographic system, it is obvious that each chromatographic system has a different k'_{opt} value. To fairly compare the optimal performance of the different chromatographic systems, each system should be evaluated at its proper k'_{opt} value. This k'_{opt} value furthermore also depends upon the phase thickness ratio ϕ [22]. For the $\phi \ll 1$ case, it has been shown by Scott that $k'_{\text{opt}} = 2.69$ for PDC in a cylindrical capillary with $d = d_{\text{opt}}$ [23]. For PDC in a flat rectangular channel (with $\phi \ll 1$ and $d = d_{\text{opt}}$), it can be shown that $k'_{\text{opt}} = 2.47$ when the side-wall effect is neglected [22], whereas $k'_{\text{opt}} = 2.92$ when the side-wall effect is taken into account. The latter result has been obtained by numerically optimizing Eq. (24), using the expression for f' given by Eq. (T4b) in Table 1. Numerically solving Eq. (25) with f' given by Eq. (T5a), yields $k'_{\text{opt}} = 0.82$ for SDC in a flat rectangular channel without side-walls. Replacing f' by the expression given in Eq. (T5b), it can be shown that the k'_{opt} value for SDC shifts to $k'_{\text{opt}} = 0.92$ when the side-wall effect is taken into account. It should be recalled that both cited k'_{opt} values are for the $\phi \ll 1$ case. For cases in which the $\phi \ll 1$ assumption is not valid, the calculated k'_{opt} value is given in the caption or legend of the corresponding figure. For HPLC, a similar k' optimization can be performed. According to Ref. [4], the k'_{opt} value for a HPLC column with $d_p = d_{p,\text{opt}}$ can be calculated to be $k'_{\text{opt}} = 2.4$.

In Fig. 6, the separation speed of liquid phase SDC is compared with that of conventional HPLC. The plain line corresponds to a HPLC separation with $k' = k'_{\text{opt}} = 2.4$ and with $u = u_{\max}$ given by Poiseuille's law ($\Delta P_{\max} = 400$ bar). The two dashed lines refer to SDC and have been calculated using Eq. (T5b). The upper dashed line is for $u_m = u_{\text{opt}}$ and $k' = 2.4$, allowing one to compare the SDC and HPLC system for the same k' value, and for approximately the same u_m value. The lower dashed line is for $u_m = 10u_{\text{opt}}$ and $k' = 0.92$, and represents the

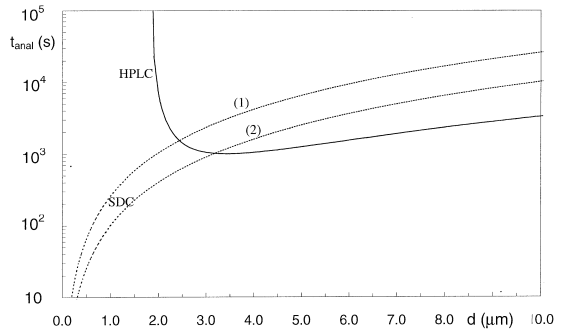

Fig. 6. Comparison of analysis times between liquid phase SDC (dashed lines) and HPLC (plain line, $k'_{HPLC,opt}=2.4$, $u=u_{max}$ for $\Delta P_{max}=400$ bar and $\psi=750$) for $R_s=1.25$ and for $\alpha_s=1.03$. For SDC, two cases are considered: (1) $k'=2.4$ and $u_m=u_{opt}$ and (2) $k'=k'_{opt}=0.92$ and $u_m=10u_{opt}$. Other parameters: $\phi_{SDC}=0.1$, $\epsilon=0.5$, $D_m=1\cdot10^{-9}$ m^2/s, $\mu=10^{-3}$ kg/(m s).

absolute minimal analysis time in SDC. The HPLC curve clearly shows the dramatic increase of the analysis time when sub-optimal particle diameters are used. The SDC curves clearly reflect the main advantage of SDC: the analysis time unconditionally decreases with the channel thickness.

Fig. 7 shows the influence of the stationary film thickness (via $\phi=\delta/d$) on the analysis time. For $\phi\ll1$, the use of very small channel thickness values leads to extremely small analysis times. With the current state of detector technology, the correspondingly small peak widths and the extremely small mass loadability of such columns will however inevitably lead to detection problems. Fig. 7 has been

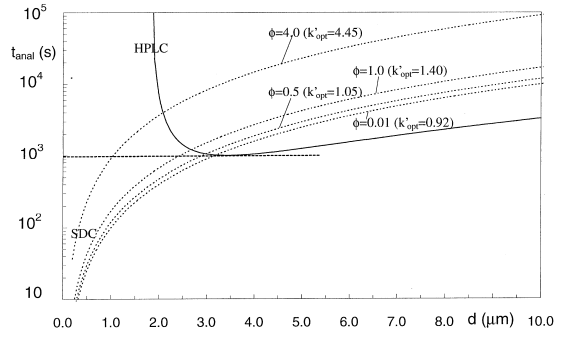

Fig. 7. Influence of the stationary phase thickness on the analysis time for liquid phase SDC, and comparison with conventional HPLC (plain line, $k'_{HPLC,opt}=2.4$). Parameter values: $R_s=1.25$, $\alpha_s=1.03$, $\epsilon=0.5$, $D_m=1\cdot10^{-9}$ m^2/s, $\mu=10^{-3}$ kg/(m s), $u_m=10u_{opt}$ (SDC), $u=u_{max}$ for $\Delta P_{max}=400$ bar and $\psi=750$ (HPLC).

included to show that, by sacrificing part of the gain in analysis time in favor of an increased film thickness, the SDC principle offers a large margin over which the film thickness (and hence the concentration detectability) can be increased before the analysis time exceeds the analysis time of the best possible HPLC column.

In Fig. 8, SDC is compared with open-tubular PDC in a flat rectangular channel. Compared to Fig. 6, the SDC now only becomes advantageous over the PDC system at much smaller d values. This is of course due to the fact that open-tubular PDC provides much faster separation kinetics than the HPLC system. Comparing the plain with the dashed lines, Fig. 8 also shows that the side-wall effect is less severe for SDC than for PDC, a fact which has already been discussed in Section 4.

In Fig. 9, the comparison with PDC is generalized over the entire range of practically relevant α_s values. First a comparison with HPLC is made (Fig. 9a). The advantage is obvious. In Fig. 9b, a comparison is made with open-tubular PDC in a cylindrical capillary. For the latter, two values of the column diameter have been considered. One, $d=5$ μm, representing the present state of the art in research laboratories [24] and corresponding to a column which exhibits exactly the same mass loadability as a 1 μm thick and 100 μm wide SDC channel (assuming $\phi=0.1$ for both cases). And one, $d=1$ μm,

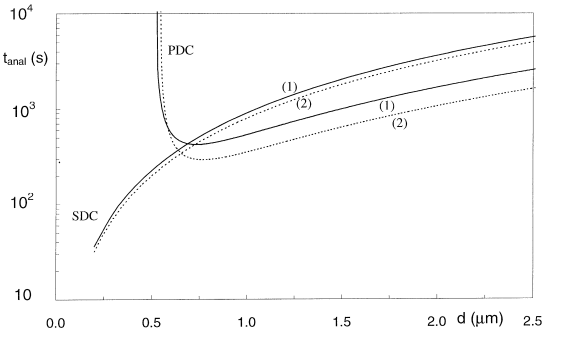

Fig. 8. Comparison of analysis times between liquid phase SDC and open-tubular LC (OT-LC) in flat-rectangular channel. Two cases are considered: (1) without side-walls (dashed lines: $k'_{OT\text{-}LC,opt}=2.47$ and $k'_{SDC,opt}=0.82$) and (2) with side-walls (plain lines: $k'_{OT\text{-}LC,opt}=2.92$ and $k'_{SDC,opt}=0.92$). Other parameters: $R_s=1.25$, $\alpha_s=1.01$, $\phi=0.1$, $\epsilon=0.5$, $D_m=1\cdot10^{-9}$ m^2/s, $\mu=10^{-3}$ kg/(m s), $u_m=10u_{opt}$ (SDC), $u=u_{max}$ for $\Delta P_{max}=400$ bar and $\psi=32$ (OT-LC).

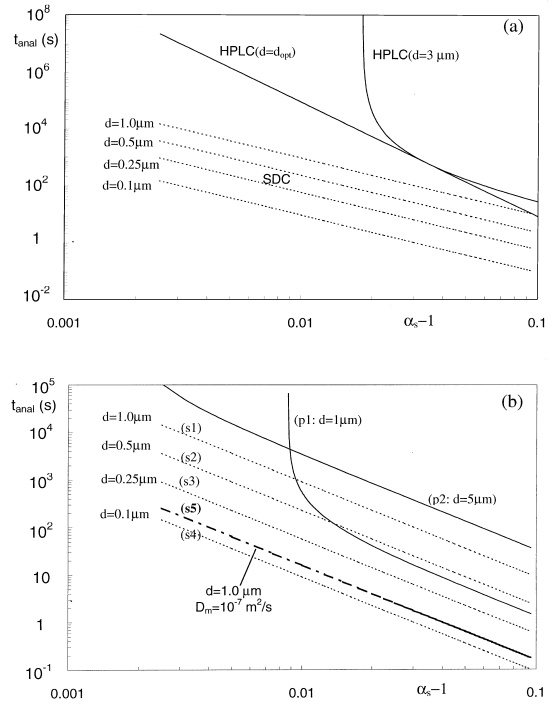

Fig. 9. Variation of t_{anal} with $\alpha_s - 1$: comparison between SDC (dashed lines) and three different types of PDC (plain lines): (a) HPLC ($\psi = 750$) and (b) OT-LC in cylindrical capillary ($\psi = 32$). Parameters: $R_s = 1.25$, $\alpha_s = 1.01$, $\phi = 0.1$, $\epsilon = 0.5$, $D_m = 1 \cdot 10^{-9}$ m^2/s, $\mu = 10^{-3}$ kg/(m s), $u_m = 10u_{opt}$ (SDC), $u = u_{max}$ for $\Delta P_{max} =$ 400 bar (PDC).

allowing us to compare with the 1-μm SDC channel under the condition of equal channel diameters. Successful measurements in a 1-μm capillary have already been successfully demonstrated in the past [25]. Analysis times corresponding to other channel diameters can easily be obtained by noting that $t_{anal} \sim d^2$. Fig. 9b clearly shows that, for the same channel thickness (compare curve p1 with curve s1), PDC yields shorter separation times than SDC in the range of large α_s. This is due to the fact that the $HETP_m$ value for PDC [Eq. (4a)] is smaller than for SDC [Eq. (3)]. In the range of small α_s on the other hand, the pressure drop limitation no longer allows to operate the PDC channel beyond or at its optimal mobile phase velocity. Instead, the mobile phase velocity has to be strongly reduced, such that, below a given value of α_s, the SDC channel yields shorter analysis times than the PDC channel.

Apart from yielding superior separation speeds in the range of small α_s, SDC also betters PDC over the entire α_s range by taking advantage of the possibility to use a smaller channel thickness (cf. curves s1–s4 in Fig. 9b). As is demonstrated by curve (s5), this reasoning should however not lead to the use of impractical thin channels. Curve (s5) shows that, by working under supercritical fluid conditions, SDC offers the possibility to generate separation speeds which are minimally 10-times larger than the separation speeds in a PDC channel with the same diameter. These extremely large separation speeds arise from the fact that the SDC principle allows to keep a uniform pressure over the entire channel length. A shear-driven SFC separation can hence be performed at pressures just above the critical pressure (typically around 40 bar), whereas in PDC the column efficiency loss caused by the axial pressure gradient [26] obliges one to operate the column at pressures which are typically in the 200 bar region, where the molecular diffusivity is about one order of magnitude smaller than near P_{crit}. Another advantage of SDC is that the supercritical fluid separations can be performed in 1 μm or even sub-1 μm channels, whereas in supercritical PDC, the very stringent pressure drop limitation imposes the use of channel diameters which are of the order of 25 to 50 μm [27]. Considering this point together with the increased molecular diffusivity, it is obvious that supercritical fluid SDC might yield analysis times which are 1000 to 5000 times smaller than for pressure-driven SFC.

As the shear-force driving principle still holds in the gas phase, it is also worthwhile to investigate the potential of shear-driven GC. Fig. 10 shows the variation of t_{anal} with ϕ in a 1 μm thick channel, for three different values of the mobile phase diffusivity and for $\alpha_s = 1.01$. Analysis times corresponding to other channel diameters can again easily be obtained by noting that $t_{anal} \sim d^2$. In the range of large ϕ values, the stationary phase mass transfer becomes the rate-determining factor and there is no influence of the mobile phase diffusivity. In the range of small ϕ values on the other hand, the beneficial influence of the increased mobile phase diffusivity becomes clearly apparent. To allow for a comparison with PDC, the best possible t_{anal} values for conventional pressure-driven HPLC and capillary GC are given as

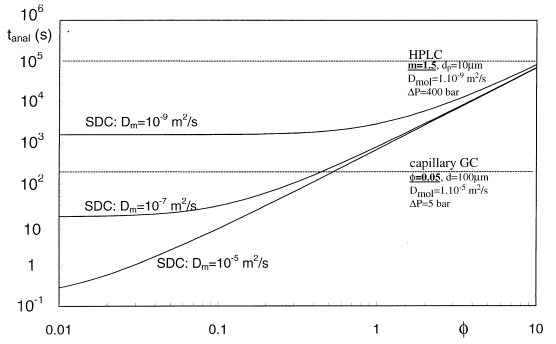

Fig. 10. SDC: variation of t_{anal} with ϕ for three different values of D_m. The horizontal dashed lines refer to conventional HPLC and capillary GC systems which have been optimized for the presently considered critical pair separation with $R_s=1.25$, $\alpha_s=1.01$. Other parameter values: $d_{SDC}=1$ µm, $D_s=5\cdot10^{-10}$ m^2/s, $\mu=10^{-3}$ kg/(m s) and $\psi=32$ (GC) and $\psi=750$ (HPLC).

well (cf. dashed horizontal lines). The potential gain offered by the SDC concept is again obvious.

5. Conclusions

Whereas pressure-driven chromatography suffers from a pressure-drop limitation, and whereas electrically-driven chromatography suffers from a voltage-drop limitation, no such theoretical limitation exists for SDC. As a consequence, the SDC principle has the potential to offer a theoretically unlimited resolution and separation speed capacity. The presently investigated flat rectangular channel configuration should allow to combine these large resolutions and separation speeds with a sufficiently large mass loadability.

In the present paper, it is shown how the theoretical HETP expression for SDC in a flat rectangular channel can be derived from Aris' general solution procedure. From this result, the advantage of SDC in terms of total achievable plate number, analysis time and/or mass loadability could be demonstrated, and this over the entire range of LC, GC and SFC conditions. For the latter, a marked additional advantage is obtained because the absence of a pressure drop completely eliminates the axial density gradient problem and the accompanying loss in resolution. This might lead to a renewed interest in SFC separations.

It should however be noted that a large number of technological hurdles still has to be taken (e.g., the need for miniaturized and fast on-column injection and detection systems) before it will be possible to exploit the SDC concept to its full extent. The advantages resulting from a pressure-drop less operation are however so obvious that they should provide the required stimulus to increase the research efforts in these fields.

6. Symbols

- C, mass transfer contribution to HETP, see Eq. (15), (s)
- d, channel thickness, column diameter, (m)
- D_m, molecular diffusion coefficient mobile phase, (m^2/s)
- D_s, molecular diffusion coefficient stationary phase, (m^2/s)
- f, g, help-functions, see Eq. (A.3)
- f', k'-dependent part of C, defined in Eq. (T2), (/)
- HETP, height equivalent to a theoretical plate, (m)
- k', retention factor, (/)
- m, capacity ratio, (/)
- n, sample solute concentration, see Ref. [13]
- N, theoretical plate number, (/)
- P, pressure, [kg/(m s^2)]
- R, ratio of void peak to retained peak residence time, see Eq. (A.6), (/)
- r_i, inner radius annular chromatographic channel system, see Ref. [13]
- R_s, resolution factor, (/)
- r, radial coordinate, (m)
- r_c, column radius, (m)
- t_{anal}, analysis time, (s)
- u, local mobile phase velocity, (m/s)
- u_m, mean mobile phase velocity, (m/s)
- $\bar{u}$, radially averaged mobile phase velocity, see Eq. (A.12), (m/s)
- w, channel width, (m)
- x, y, z, spatial coordinates, (m)

6.1. Roman symbols

- u, u_m, dimensionless velocities (/)
- y, dimensionless thickness coordinate (/)

6.2. Greek symbols

- α_s, separation factor (/)
- δ, stationary phase thickness, (m)
- ΔP, pressure drop (bar)
- ϕ, film thickness ratio ($\phi = \delta/d$) (/)
- κ, Aris coefficient, see Eq. (A.5) (/)
- μ, dynamic viscosity [kg/(m s)]
- ψ, flow resistance factor, $\psi = 32$ (cylindrical capillary) and $\psi = 12$ (channel with flat rectangular cross-section) (/)
- χ, auxiliary function, see Eq. (A.1) (/)

6.3. Subscripts

- in, channel inlet conditions
- m, mobile phase
- min, minimum
- opt, optimum
- out, channel outlet conditions
- s, stationary phase
- sw, side-wall

Acknowledgements

The authors greatly acknowledge Professor H. Poppe for revising the calculations and for his stimulating comments and J.-P. Chervet (LC Packings) for helping out with the preliminary flow tracer experiments.

A.1. Calculation of $HETP_m$ for SDC flow between two flat parallel plates

Departing from the reference coordinate framework in Fig. 3a, Aris' general solution procedure [13] first requires the introduction of an auxiliary function χ:

$$\chi(y) = u(y) - u_m \tag{A.1}$$

For the flow field depicted in Fig. 3a, it can easily be verified that:

$$\chi(y) = 2 - 2y \; (0 \le y \le 1) \tag{A.2a}$$

$$= 2 + 2y \; (-1 \le y \le 0) \tag{A.2b}$$

The calculation further requires the introduction of two other auxiliary functions f and g [13]. For a flow system with a space-independent diffusion coefficient, these functions are respectively given by:

$$\frac{d^2 f}{dy^2} = 1 - \chi, \text{ with } \frac{df}{dy} = 0 \text{ at } y = 0 \tag{A.3a}$$

$$\frac{d^2 g}{dy^2} = -1, \text{ with } \frac{dg}{dy} = 0 \text{ at } y = 0 \tag{A.3b}$$

Using the above definitions, the mobile-phase mass transfer contribution ($HETP_m$) in a channel with radius r_c is, according to Ref. [13], given by:

$$HETP_m = 2\kappa u_m \cdot \frac{r_c^2}{D_m} \tag{A.4}$$

with:

$$\kappa = \kappa_1 + 2(1 - R)\kappa_2 + (1 - R)^2 \kappa_3 \tag{A.5a}$$

and

$$\kappa_1 = \frac{1}{2} \cdot \int_{-1}^{1} \left[\frac{df}{dy} \right]^2 \cdot dy \tag{A.5b}$$

$$\kappa_2 = \frac{1}{2} \cdot \int_{-1}^{1} \left[\frac{df}{dy} \cdot \frac{dg}{dy} \right] \cdot dy \tag{A.5c}$$

$$\kappa_3 = \frac{1}{2} \cdot \int_{-1}^{1} \left[\frac{dg}{dy} \right]^2 \cdot dy \tag{A.5d}$$

In Eq. (A.5a), R represents the ratio of the retention time of the unretained void peak to that of a given retained peak:

$$R = \frac{1}{1 + k'} \tag{A.6}$$

For the flow system depicted in Fig. 3a, the channel radius r_c corresponds to one half of the distance between the two stationary walls, and is hence given by:

$$r_c = d \tag{A.7}$$

Considering the expression for χ, solving Eq. (A.3a) yields:

$$\frac{df}{dy} = -y + y^2 \ (0 \le y \le 1) \quad \text{and}$$
$$\frac{df}{dy} = -y - y^2 \ (-1 \le y \le 0) \tag{A.8a}$$

Solving Eq. (A.3b) yields:

$$\frac{dg}{dy} = -y \tag{A.8a}$$

Using these expressions, and calculating κ_i ($i=1$, 3) according to Eq. (A.5), it is found that:

$$\kappa = \frac{1}{30} + 2(1-R)\cdot\frac{1}{12} + (1-R)^2\cdot\frac{1}{3} = \frac{32 - 50R + 20R^2}{60} \tag{A.9}$$

Replacing R by its relation to k' then finally yields:

$$\mathrm{HETP_m} = \frac{2}{30}\cdot\frac{1 + 7k' + 16k'^2}{(1+k')^2}\cdot u_m \cdot \frac{d^2}{D_m} \tag{A.10}$$

A.2. Calculation of $HETP_m$ for SDC flow in a flat rectangular channel with finite lateral width

Considering a flat rectangular channel in which the upper channel wall is moving with velocity $=u_w$, while the channel bottom wall and the side-walls are at rest, and considering the coordinate reference frame defined in Fig. 5a, it can be shown that the velocity field of the resulting SDC flow is given by:

$$u(z,y) = \frac{4u_w}{\pi}\cdot\sum_{n=0}^{+\infty}\frac{1}{2n+1}\sin\left[(2n+1)\frac{\pi}{w}\left(z+\frac{w}{2}\right)\right] \cdot \frac{\sinh\left[(2n+1)\frac{\pi}{w}\left(y+\frac{d}{2}\right)\right]}{\sinh\left[\frac{(2n+1)\pi d}{w}\right]} \tag{A.11}$$

The validity of Eq. (A.11) can be verified from its ability to satisfy the corresponding Navier–Stokes equation and the prescribed boundary conditions, and also from the analogy with the equivalent problem of finding the temperature distribution in an infinite rectangular rod with one side kept at $T=T_w$ and with the other three sides kept at $T=0$. The solution for this problem can be found in most basic heat transfer text books [28].

Averaging now the velocity profile over the y-direction:

$$\bar{u}(z) = \frac{1}{d}\cdot\int_{-d/2}^{d/2} u(z,y)\cdot dy \tag{A.12}$$

$$\bar{u}(z) = \frac{4u_w}{\pi^2}\cdot\frac{w}{d} \cdot\sum_{n=0}^{+\infty}\frac{1}{(2n+1)^2}\sin\left[(2n+1)\frac{\pi}{w}\left(z+\frac{w}{2}\right)\right] \cdot\frac{\cosh\left[(2n+1)\pi\frac{d}{w}\right]-1}{\sinh\left[\frac{(2n+1)\pi d}{w}\right]} \tag{A.13}$$

and putting:

$$F(n) = \frac{\cosh\left[(2n+1)\pi\frac{d}{w}\right]-1}{\sinh\left[\frac{(2n+1)\pi d}{w}\right]} \tag{A.14}$$

it can be verified that the cross-section averaged mobile phase velocity u_m is given by:

$$u_m = \frac{1}{w}\cdot\int_{-w/2}^{w/2}\bar{u}(z)\cdot dz = \frac{8u_w}{\pi^2}\cdot\frac{w}{d}\cdot\sum_{n=0}^{+\infty}\frac{1}{(2n+1)^3}\cdot F(n) \tag{A.15}$$

The expressions obtained for $\bar{u}(z)$ and u_m are schematically represented in Fig. 5b. The gain obtained from the above manipulations is that the 2D flow dispersion problem (in the y,z-direction) has been transformed into a 1D flow dispersion problem (in the z-direction), such that it can be solved [20] according to the procedure described in Section A.1. In the present case, Aris' general solution procedure only requires the calculation of the f-help function given in [29]:

$$\frac{d^2f}{dz^2} = 1 - \chi(z), \quad \text{with } \chi(z) = 1 - \frac{\bar{u}(z)}{u_m} \text{ and}$$
$$\frac{df}{dz} = 0 \text{ at } z = 0 \tag{A.16}$$

Solving Eq. (A.16) yields:

$$\frac{df}{dz} = z - \frac{1}{u_m}\cdot\int_{-w/2}^{z}\bar{u}(z')\cdot dz' \tag{A.17}$$

Replacing $\bar{u}(z')$ by the expression given in Eq. (A.13), Eq. (A.17) yields:

$$\frac{df}{dz} = z - \frac{1}{u_m} \cdot \frac{4u_w}{\pi^3} \cdot \frac{w^2}{d} \cdot \sum_{n=0}^{+\infty} \frac{1}{(2n+1)^3} \cdot \cos\left[(2n+1)\frac{\pi}{w}\left(z+\frac{w}{2}\right)\right] \cdot F(n) \quad \text{(A.18)}$$

From Eq. (A.17), the κ_{sw} value can be directly calculated according to [20]:

$$\kappa_{sw} = \frac{1}{w} \cdot \int_{-w/2}^{w/2} \left[\frac{df}{dz}\right]^2 \cdot dz \quad \text{(A.19a)}$$

This expression has been numerically evaluated, yielding:

$$\kappa_{sw} = 0.0989 \quad \text{(A.19b)}$$

As the summation series given in Eq. (A.18) converges only very slowly, it was found to be necessary to include at least 20 000 terms in order to have a result which is sufficiently accurate on the fourth digit. According to Ref. [20], the additional $HETP_{m,sw}$ contribution to the peak broadening can now be calculated as:

$$HETP_{m,sw} = 2\kappa_{sw} u_m \frac{(d/2)^2}{D_m} = 0.04945 u_m \cdot \frac{d^2}{D_m} \quad \text{(A.20)}$$

References

[1] G.J.M. Bruin, P.P.H. Tock, J.C. Kraak, H. Poppe, J. Chromatogr. 517 (1990) 557–572.
[2] J.E. Mac Nair, K.C. Lewis, J.W. Jorgenson, Anal. Chem. 69 (1997) 983–989.
[3] J.E. Mac Nair, K.D. Patel, J.W. Jorgenson, Anal. Chem. 71 (1999) 700–708.
[4] E.D. Katz, K. Ogan, R.P.W. Scott, in: F. Bruner (Ed.), The Science of Chromatography, Journal of Chromatography Library, Vol. 32, Elsevier, Amsterdam, 1985, pp. 403–434.
[5] G. Guiochon, J. Chromatogr. 185 (1979) 3–26.
[6] M.M. Dittmann, K. Wienand, F. Bek, G.P. Rozing, LC·GC 13 (1995) 800–814.
[7] R.H. Sabersky, A.J. Acosta, E.G. Hauptmann, in: Fluid Flows – A First Course in Fluid Mechanics, Collier McMillan, London, 1971, p. 223.
[8] G. Desmet, G. Baron, Eur. Pat. Appl. text no. 97201699.2 (1997).
[9] S.Y. Chou, Proc. IEEE 85 (1997) 652–671.
[10] S.Y. Chou, private communication.
[11] J.C. Giddings, J.P. Chang, M.N. Myers, J.M. Davis, K.D. Caldwell, J. Chromatogr. 255 (1983) 359–379.
[12] T. Tsuda, J.V. Sweedler, R.N. Zare, Anal. Chem. 62 (1990) 2149–2152.
[13] R. Aris, Proc. Royal Soc. A 252 (1959) 538–550.
[14] H. Schlichting, Boundary-Layer Theory, McGraw Hill, London, 1958.
[15] J.C. Giddings, J. Chromatogr. 5 (1961) 46–60.
[16] J.E. Golay, J. Chromatogr. 216 (1981) 1–8.
[17] M.R. Doshi, P.M. Daiya, W.M. Gill, Chem. Eng. Sci. 33 (1978) 795–804.
[18] P.C. Chatwin, P.J. Sullivan, J. Fluid Mech. 120 (1982) 347–358.
[19] M. Martin, J.-L. Jurado-Baizaval, G. Guiochon, Chromatographia 16 (1982) 98–102.
[20] A. Cifuentes, H. Poppe, Chromatographia 255 (1994) 391–404.
[21] J.H. Knox, M.T. Gilbert, J. Chromatogr. 186 (1979) 405–418.
[22] G. Desmet, G.V. Baron, (1999) submitted to J. Chromatogr. A.
[23] R.P.W. Scott, J. Chromatogr. 517 (1990) 297–304.
[24] H. Poppe, in: E. Heftmann (Ed.), Chromatography, Part A: Fundamentals and Techniques, 5th ed., Journal of Chromatography Library, Vol. 51A, Elsevier, Amsterdam, 1992, pp. 151–225.
[25] C.A. Monnig, D.M. Dohmeier, J.W. Jorgenson, Anal. Chem. 63 (1991) 807–810.
[26] P.A. Peaden, M.L. Lee, J. Chromatogr. 259 (1983) 1–16.
[27] L.G. Blomberg, M. Demirbrüker, I. Hägglund, P.E. Andersson, Trends Anal. Chem. 13 (1994) 126–137.
[28] F.M. White, Heat and Mass Transfer, Addison Wesley, Reading, MA, 1988.
[29] R. Aris, Proc. Royal Soc. A 235 (1956) 67–77.